ELSEVIER

Nuclear Instruments and Methods in Physics Research A 435 (1999) 408–422

NUCLEAR INSTRUMENTS & METHODS IN PHYSICS RESEARCH Section A

www.elsevier.nl/locate/nima

Measurements of the photon detection inefficiency of calorimeters between 185 and 505 MeV

S. Ajimura[a], T. Endo[b], T. Inagaki[c,*], S. Itoh[d], Y. Kuno[c], K. Maeda[b], K. Maruyama[e], T. Nakano[a], H. Okuno[f], T. Sato[c], T. Shinkawa[c], T. Suda[b], K. Sugiyama[a], T. Terasawa[g], A. Toyofuku[b]

[a]*Department of Physics, Osaka University, Osaka 560, Japan*
[b]*Department of Physics, Tohoku University, Sendai 980, Japan*
[c]*High Energy Accelerator Research Organization (KEK), 1-1 Oho, Tsukuba 305, Japan*
[d]*The Institute of Physical and Chemical Research, Wako 351-01, Japan*
[e]*Center for Nuclear Study, University of Tokyo, Tanashi, Tokyo 188, Japan*
[f]*KEK, Tanashi-branch, Tanashi, Tokyo 188, Japan*
[g]*Laboratory of Nuclear Science, Tohoku University, Sendai 982, Japan*

Received 29 January 1998; received in revised form 7 May 1999; accepted 15 May 1999

Abstract

The detection inefficiencies for photons of total-absorption-type electromagnetic calorimeters, an undoped CsI crystal counter and a lead-scintillator sandwich counter, have been measured at photon energies (E_γ) between 185 and 505 MeV with the tagged photon beam from the INS-ES. The effect of punch-through is estimated by an EGS calculation. The other source of inefficiency, the photonuclear interaction effect, is examined after the interaction is identified by neutron signals observed with liquid scintillation counters surrounding the sample calorimeter. The inefficiency due to the photonuclear interaction in the case of the CsI calorimeter at 1-MeV threshold is found to be 10^{-5}–10^{-6} and shows a monotonic decrease with E_γ. The detection inefficiency of the sandwich calorimeter is found to be dominated by the sampling effect after photonuclear interactions.

PACS: 29.40Vj

Keywords: Calorimeter inefficiency; Tagged photon beam; First-nucleon-resonance region

1. Introduction

It is crucial to know the detection inefficiency of calorimeter for photons in some high-energy experiments such as the measurement of the $K_L^0 \to \pi^0 \nu\bar{\nu}$ decay branching ratio [1]. In this experiment the decay will be identified as $\pi^0 +$ *nothing*, where *nothing* means no emission of visible particles. So, no association of other particles should be detected with a high efficiency.

This paper describes the first dedicated measurement of the detection inefficiency for photons, while those for charged particles were reported elsewhere [2].

* Correponding author.
E-mail address: inagaki@kekvax.kek.jp (T. Inagaki)

0168-9002/99/$ - see front matter
PII: S0168-9002(99)00571-9

Three processes are sources of inefficiency for photons in a total-absorption-type electromagnetic calorimeter. The first is the punch-through when a photon penetrates the calorimeter without any interactions. Since the electromagnetic cascade shower process is a dominant process for photons, the probability of the punch-through could be evaluated with the electromagnetic cascade shower code, EGS [3]. However, since the punch-through for a total-absorption-type calorimeter is a tiny effect, the validity of the estimation has to be experimentally examined.

The second source is photonuclear interaction. When a photonuclear interaction takes place in the calorimeter ahead of an electromagnetic cascade shower and secondary particles produced by the interaction do not generate any large signals above the detection threshold, it causes a detection inefficiency. In this case the secondaries may be neutrons or the charged particles with low energies below the detection threshold. A numerical evaluation of the detection inefficiency due to the photonuclear interaction is more difficult than that due to the punch-through. The total photonuclear cross section for calorimeter materials can be calculated from the experimental data which have been measured at various energies for several nuclei, and then the ratio of the strength of photonuclear and electromagnetic interactions can be estimated with little ambiguity. However, it is not possible to know about secondaries after the photonuclear interaction together with the calorimeter response for these particles. Since no realistic simulation code exists, the detection inefficiency due to the photonuclear interaction should be experimentally estimated.

The third is the sampling effect which arises in the case of a sampling calorimeter such as a lead-scintillator sandwich counter. The sampling effect could be divided into two according to the type of the interaction process. One is the electromagnetic cascade shower process such as a multi-step Compton scattering where all tracks of secondary electrons are confined within the converter (non-active). This can be also estimated from an EGS calculation. The other is a photonuclear interaction followed by the absorption of the secondaries in the converter, and the effect cannot be reliably evaluated by any calculations.

In the photon energy (E_γ) region from a few MeV to GeV, the photonuclear interaction cross section drastically changes its behavior in contrast with that of the electromagnetic cascade shower process. Around 20 MeV the photonuclear interaction cross section is as large as a few percent of that of the electromagnetic cascade shower process due to the giant dipole resonance, and then it rapidly decreases with E_γ. However, below the pion-production threshold ($E_\gamma < 140$ MeV) there are a lot of cross-section data of the $\sigma(\gamma, n's)$ reactions and then the detection inefficiency can be estimated using the data [4,5] with a small correction for the emission of visible particles. It is because emissions of charged particles, protons, d or α are suppressed by the Coulomb barrier. On the other hand above the pion threshold ($E_\gamma > 140$ MeV) the dominant process is the pion production. The cross section rises due to the excitation of the nucleon resonances up to 0.1% level of the electromagnetic cascade shower cross section. Since the produced pions are visible in the calorimeter and many of recoil protons have energies high enough to penetrate the Coulomb barrier, the detection inefficiency would be smaller than the value simply calculated from the cross-section ratio between the photonuclear and electromagnetic cascade shower processes. This effect cannot be easily estimated without knowing the details about secondaries. The detection inefficiency must be evaluated by an experiment especially in this region. Since the number of visible particles produced by an interaction increases with E_γ, the detection inefficiency is expected to decrease with E_γ. This is the reason why the first nucleon resonance (Δ resonance) region is selected in the present measurement as the most important region.

For the measurement we use a tagged photon beam: photons are produced via the bremsstrahlung process in which recoil electrons are measured with a magnet spectrometer. After several tests prior to the present experiment it was found impossible to get a high-purity beam (the tagged photon beam with a high tagging efficiency) enough to measure directly the detection inefficiency at a 10^{-5} level. For the direct measurement it is required that the photon exists just at the calorimeter for each tagging signal with a probability higher

than the detection efficiency which we want to measure. However, unfortunately in the present tagging method there are several processes which cause a large miss-tagging (a swing-and-miss) rate as illustrated in Fig. 1: (a) low-energy beam electrons as a halo, (b) a two-step interaction in the radiator to produce e^+e^- which are swept away by an analyzer magnet, (c) the tagged photon emitted in a large angle outside the acceptance of the sample calorimeter due to a Coulomb scattering of the incident electron in the radiator, etc. It is hard to reduce at once these processes causing the miss-tagging: for examples, a thicker radiator is required against (a) but it enhances (b) and (c).

In the present experiment a large volume of liquid scintillator surrounds the sample calorimeter. At first most of miss-tagging can be reduced by requiring a signal in the liquid scintillator which coincides with the tagging signal. Moreover, the liquid scintillator can select neutron to identify photonuclear interactions. Since a large number of neutrons (more than 10) are expected to emerge after a photonuclear interaction, at least one of them can be efficiently detected with the liquid scintillator of a large volume. The identification of the photonuclear interaction could be checked overall by a comparison with the existing data of the total photonuclear interaction cross section.

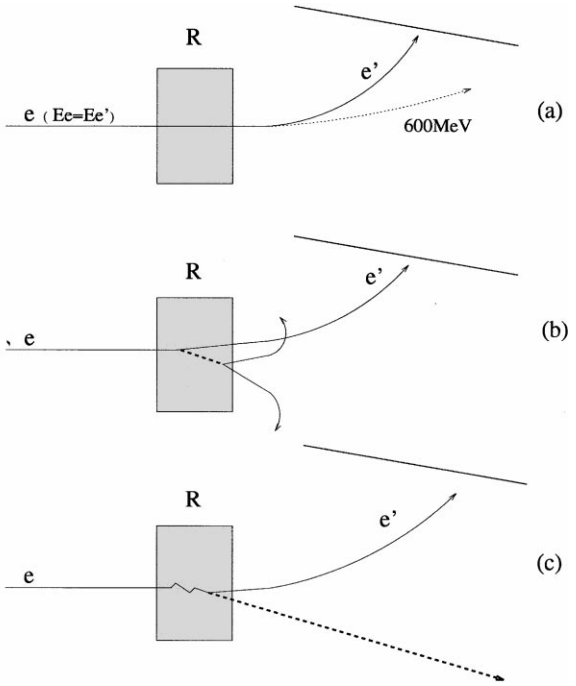

Fig. 1. Processes to cause the miss tagging: (a) low-energy beam electrons, (b) two-step interactions in the radiator and (c) large-angle emission of photons. e, e′ and R are the incident electron, the scattered one and the radiator, respectively.

2. Experimental method

The experiment has been carried out with the photon tagging system [6] at the electron synchrotron of the Institute for Nuclear Study (INS-ES). The setup is essentially divided into two: the tagging and sample calorimeter systems, as shown in Fig. 2. Incident electrons extracted from the INS-ES at the peak energy of 600 MeV hit a radiator of an aluminum foil of 0.35 mm thick (3.9×10^{-3} radiation length), and produce bremsstrahlung photons. Since the INS-ES is operated with a resonance excitation, the beam energy varies sinusoidally by about 5% in a beam duration for a 10% duty factor. The energy variation is compensated by synchronously adjusting the field of the beam-line magnets to keep the beam trajectory at the right position [7] and the incident electron energy for each photon can be calculated in an off-line analysis from information of the beam timing with respect to the excitation of the synchrotron magnets.

Scattered electrons after bremsstrahlung are bent by an analyzer magnet and detected with two sets of hodoscopes consisting of 32 and 8 scintillation counters. The former 32 counters (tagging counters) are placed along the focal line of the analyzer magnet with respect to the radiator and cover a momentum range of 95–415 MeV/c with an acceptance of $\pm$ 5 MeV/c for each counter. Each of the eight scintillation counters is a backing counter for every four tagging counters. A coincidence signal between a tagging counter and a corresponding backing counter is called 'tag-signal'. Since the recoil energy to the radiator atoms is negligibly small, the photon energy E_γ is given as $E_\gamma = E_0 - E_e$ in a good approximation, where E_0 and E_e are the energies of the incident and scattered electrons,

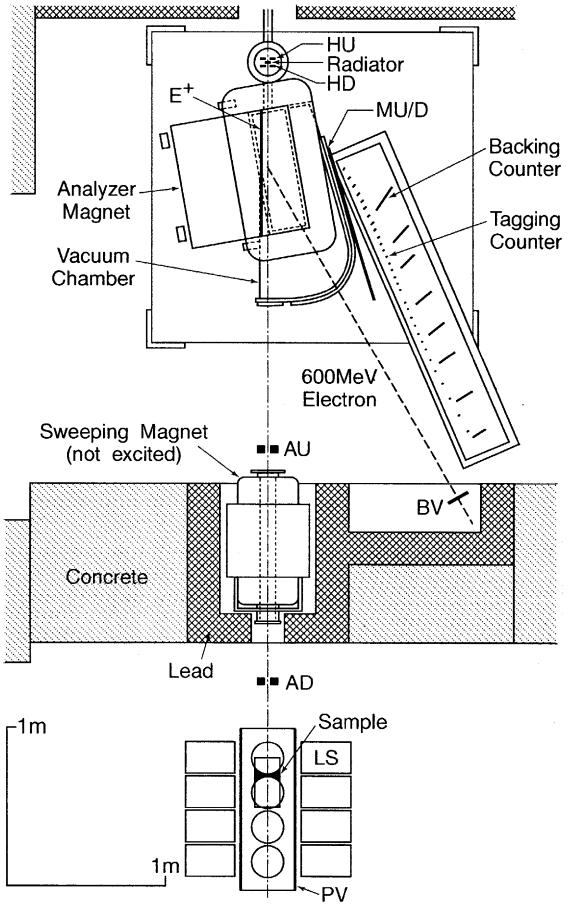

Fig. 2. Plan-view of the experimental setup. The veto-counters, HU/D, E^+, MU/D, BV and AU/D are installed to reduce miss-tagging and the details of their aims are described in the text.

respectively. E_γ is determined (tagged) by a 10-MeV step over the range from 185 to 505 MeV. Details of the INS-ES tagging system are reported in [6,7].

Two types of calorimeters are prepared as the sample calorimeter to study the detection inefficiency for photons. One is an undoped-CsI-crystal calorimeter of 30-cm thick (about 16 radiation length). It consists of 10 blocks (one center block and nine side blocks) which are tightly packed as shown in Fig. 3. The light output is directly read from the back (downstream) by a $1\frac{1}{8}$-in diameter photomultiplier tube (PMT) for each side-block and a 2-in PMT for the center block. The lateral

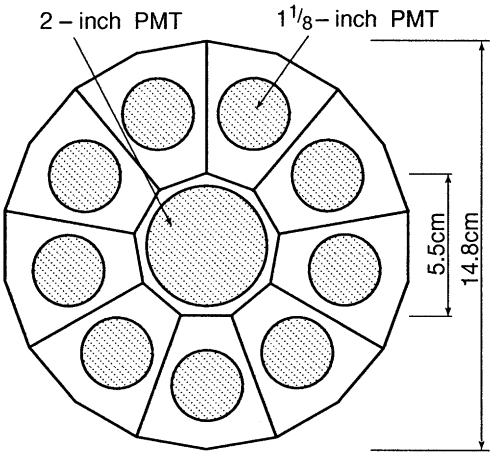

Fig. 3. Front view of the CsI calorimeter.

radius of the whole assembly is 7.4 cm, about twice the Moliére-radius. The other is a lead-scintillator sandwich calorimeter with 41 layers of 6-mm thick hexagonal plastic scintillator plates intervened by 2-mm thick lead plates as shown in Fig. 4. The light is read from the sides of the hexagon by six 2-in PMTs via six wave-length-shifter bars. The sandwich counter is contained in a stainless-steel pipe of 2-mm thick.

Twelve modules of the liquid scintillator (LS) surround the sample calorimeter. Four modules on each of the up-, right- and left-side direct the sample calorimeter as shown in Fig. 2 and 5. Each module of 10-l liquid scintillator (NE213) in an aluminum vessel of 200-mm in diameter and 330-mm in length is viewed by a 5-in PMT. Three long plastic scintillators (PV) 10-mm thick are placed to detect charged particles on the sample side of the liquid scintillator modules. Each one covers four LS

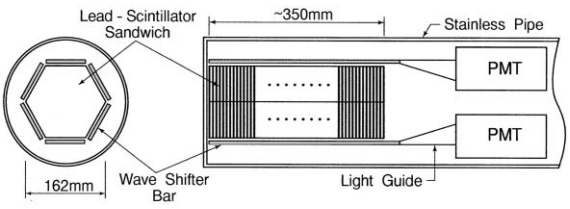

Fig. 4. Lead-scintillator sandwich calorimeter. Six 2-in PMT view the scintillators through the wave shifter bars.

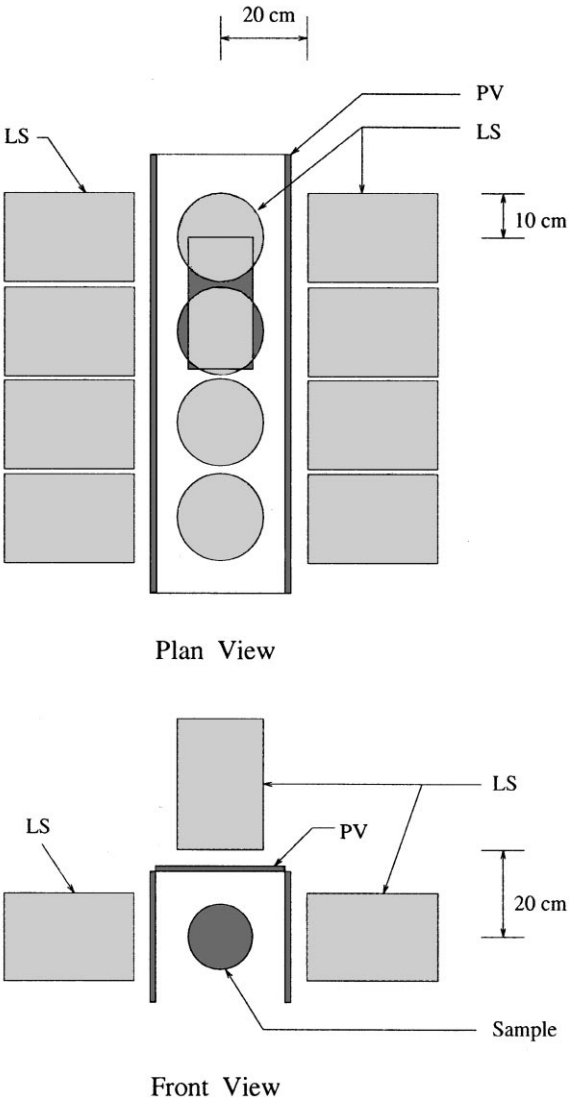

Fig. 5. Setup around the sample calorimeter. PV is three 1m-long plastic scintillation couters 10 mm thick and LS is twelve counters each of which contains about 10 l liquid scintillator.

modules on each side of the sample calorimeter and the PV signal is read from both ends.

The sample calorimeter system is placed at a distance of 4-m from the radiator. Materials between the radiator and the sample calorimeter are 1.5-m air of 10^{-2} Torr, a Mylar sheet of 250-μm thickness and 2.5-m air of atmospheric pressure.

In order to reduce the miss-tagging rate various veto-counters are installed in the tagging system as indicated in Fig. 2. Although the miss-tagging cannot be eliminated down to the level of 10^{-5}, it is very important to reduce it as low as possible. This can be clearly understood when we consider the accidental coincidence between a tag-signal and an LS-signal, which would seriously affect the detection inefficiency measurement. The low rate of miss-tagging means that a tag-signal identifies a photon with high probability. The tag-signal which accidentally associates a background LS signal hardly gives a zero-signal in the sample calorimeter, which contributes to the inefficiency. The accidental coincidences change only slightly the normalization number that is a denominator in the evaluation of the inefficiency. The low rate of miss-tagging is especially important, when we use a large-volume liquid scintillator.

Two hole counters (HU and HD) of plastic scintillator sandwich the radiator to reject the beam halo. A long plastic scintillator (E^+) is set in the magnet on the other side of the tagging counters with respect to the beam axis. These HU, HD and E^+ are installed in the vacuum chamber. A pair of long plastic scintillation counters (MU and MD) which cover the tagging counter region are set at the exit of the magnet to define the vertical acceptance of the tagging counters as 3 cm instead of their size of 5 cm (the gap of the magnet is also 5 cm). In front of the beam dump for 600 MeV electrons a plastic scintillation counter (BV) of 10-cm^2 is placed. A pair of hole counters which are made of undoped CsI are placed along the photon beam axis. The dimensions of the upstream (AU) and downstream (AD) counters are 6 (thick) × 10 (high) × 12 (wide) cm^3 with a hole of 3-cm diameter and 5 (thick) × 10 (high) × 20 (wide) cm^3 with a hole of 2-cm diameter, respectively. The AD is placed at a position 37-cm upstream from the face of the sample calorimeter in the case of the ordinary position of the sample calorimeter and AU is placed 1.5-m upstream from AD.

The PMT outputs of the veto-counters, LS and PV are fed to ADCs and the signals of the sample calorimeter are fed to double ADCs (LeCroy 2249A) of high and low ranges. The ratio of the ranges is 1:10. The PMT gains of the sample

calorimeters are adjusted by using an electron beam of 600 MeV to be 1.5-ch/MeV (for CsI) and 1-ch/MeV (for sandwich) for the high-range ADC. The electron beam with the energy spread less than 1% and the spot size of 3-mm in diameter can be provided by removing the radiator and turning off the excitation of the analyzer magnet. The PMT gain of the LS and the PSD (Pulse-Shape-Discriminator, CAMBERA-2160) equipped to every two LS modules is calibrated several times during the experiment by using checking sources of ^{60}Co and Am/Be. The threshold of the discriminator for the LS is 0.1-MeV equivalent to electrons. The time differences of all PMT signals from the trigger signal are measured by TDC.

Except for special check-runs we have taken data with the trigger which only requires the tag-signal with anti-coincidences of all veto-counters. The accelerator has been stably operated during the data acquisition. The rates of the incident electrons and the tag- and LS-signals are around 1.5k/spill (300 kHz), 5/spill (1 kHz) and 3/spill (0.6 kHz), respectively. The values shown in the parentheses are the instantaneous rates for a duty-factor of 10%, which has been carefully kept in the operation.

3. Results for the CsI calorimeter

The photon energy, E_γ, is determined by the hit tagging-counter number with a correction for the change of the incident electron energy with the extraction timing. The gain of the sample calorimeters is finally calibrated by the tagged photon beam in an off-line analysis. Since a temperature dependence of the gain of the CsI is observed, the gain calibration is performed several times using real data to compensate the variation. The gain of the sandwich calorimeter is also calibrated with tagged photons. We call these energy calibrated ADC values as E_{CsI} and E_{Sand}. The E_{CsI} and E_{Sand} correspond to the relative energy deposit in the calorimeters for which the response peaks are normalized to E_γ.

A lego plot of E_γ vs. E_{CsI} in Fig. 6 shows a good correlation between E_γ and E_{CsI}. The height shows a $1/E_\gamma$ spectrum which is consistent with bremsstrahlung. Fig. 7 shows a tagging-counter-number dependence of the miss-tagging rate, $N(E_{\mathrm{CsI}} < 1\ \mathrm{MeV})/N(\mathrm{all})$, where $N(E_{\mathrm{CsI}} < 1\ \mathrm{MeV})$ is the number of events whose E_{CsI} are less than 1 MeV and N(all) the total count of every tagging counter. The miss-tagging rate increases at both ends, which indicates that the contamination from secondary electrons with the momenta outside the

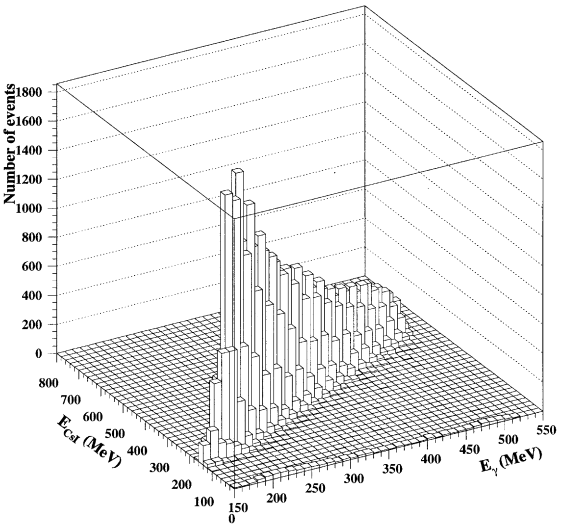

Fig. 6. E_γ vs E_{CsI} correlation.

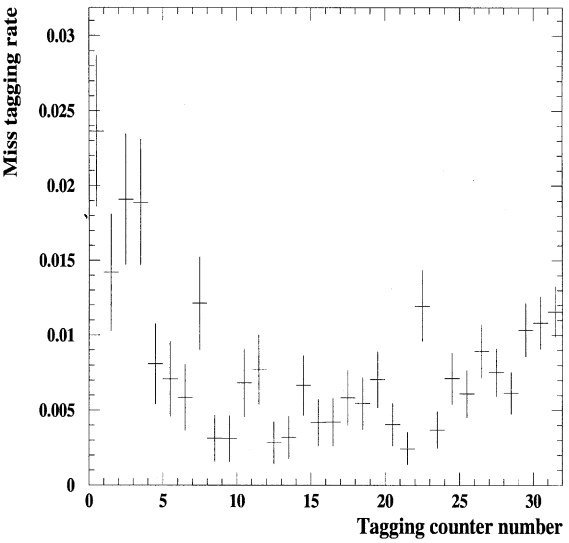

Fig. 7. Tagging-counter-number dependence of the miss tagging rate.

tagging counter acceptance is large. Anyhow the miss-tagging rate is suppressed to be less than 2%.

3.1. Analysis of tail region

A typical E_{CsI} distribution of the selected events at $E_\gamma = 250 \pm 20$ MeV is shown in Fig. 8. In order to study the data with low E_{CsI} we select the events in the region of $E_{CsI}/E_\gamma < 0.45$ (tail events). The CsI -TDC data (for the central block, t_{CsI}) of the tail events suggest the existence of two components as shown in Figs. 9(a) and (b), which are a two-dimensional plot of t_{CsI} and E_{CsI} and its distribution projected onto the t_{CsI} axis, respectively. Since the PV which is placed in front of the LS can measure the hit position along the beam axis and is sensitive to photons and neutrons slightly as well as to charged particles, we select the events with a signal in PV and evaluate the hit position using the time difference between the up- and down-stream PMTs. t_{CsI} and the hit position on the PV show correlations as shown in Figs. 10(a) and (b). Fig. 10(a) is a plot of all sample events including the peak region and 10(b) is that of the tail events. Although a single cluster is observed for all sample events which are dominated by the events in the peak region, two clusters of events are seen in the tail region: late-upstream and early-downstream.

The two-cluster structure can be explained as follows by using Fig. 11. Incident photons start electromagnetic cascade showers at various depths as shown in Fig. 11(a). The energy deposit depends on the depth of the shower-start as schematically depicted in Fig. 11(b). Therefore, as far as the cascade shower is concerned, the events in the tail region are those converted at a deep position beyond B in Fig. 11(a) where the incident photon penetrates almost through the calorimeter (punch-through). On the other hand energy deposit can be also reduced by photonuclear interaction. Since the rate of the photonuclear interaction is proportional to the number of incident photons which decreases with the depth, most events with photonuclear interactions appear in the upstream position of the calorimeter as shown in Fig. 11(c). Consequently, two components in different positions are to be observed in the tail region. In the case of the CsI calorimeter, the light velocity in CsI is low due to

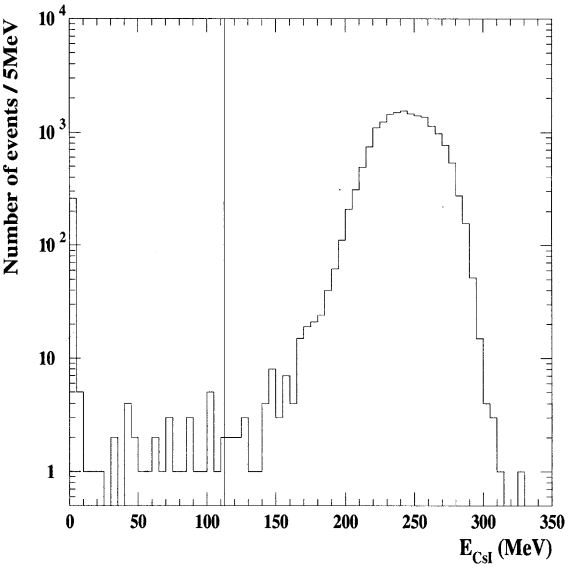

Fig. 8. E_{CsI} distribution at $E_\gamma = 250 \pm 20$ MeV. The line indicates the upper bound of the tail events for $E_\gamma = 250$ MeV data.

the high refractive index, and a time difference appears for different positions of the light source as shown in Fig. 11(d). This is the reason why we see two clusters in Fig. 10(b). The early-downstream cluster corresponds to the electromagnetic cascade shower process almost near to the punch-through, and the late-upstream one to the photonuclear interaction.

3.2. Punch-through

According to the speculation the early-cluster events with -4 ns $< t_{CsI} < -1$ ns are compared to those obtained from an EGS calculation as shown in Fig. 12. The data are well reproduced by the calculation which is normalized to the number of incident photons. It should be reminded that the real event is selected by using t_{CsI} in which the energy deposit is required to be above the threshold (2-MeV electron equivalent). On the other hand the calculated histogram shows an enhancement below 1-MeV which corresponds to the punch-through. The agreement above the threshold justifies our method to use the EGS in the estimation of the punch-through. Table 1 shows the detection

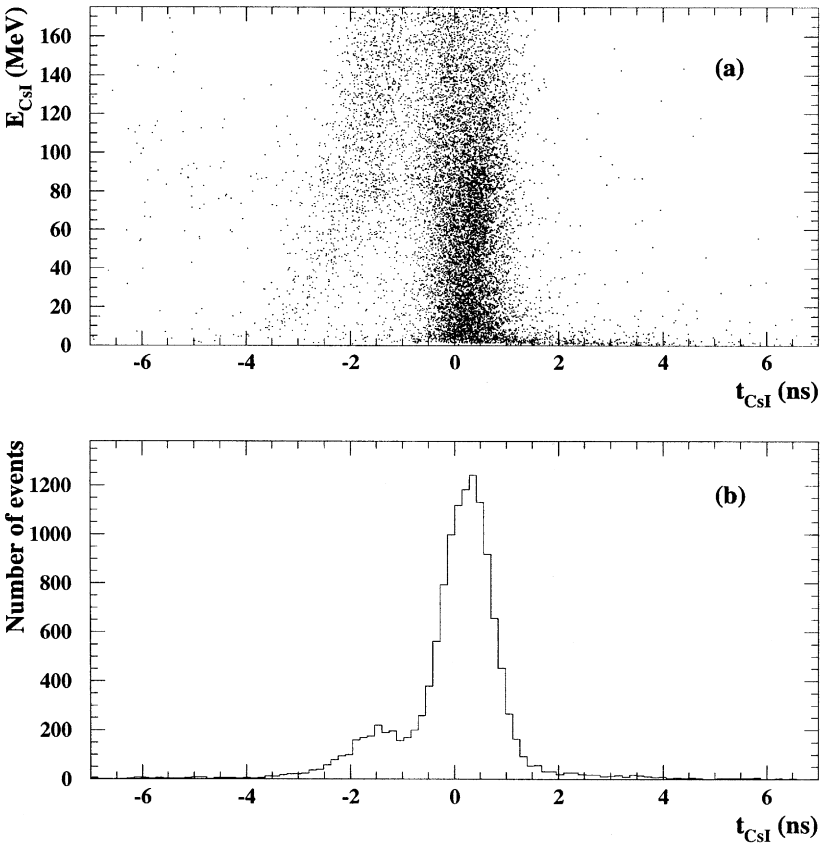

Fig. 9. Time information of the CsI calorimeter signals (t_{CsI}) for the tail events: (a) a two-dimensional plot of t_{CsI} vs E_{CsI} and (b) its projected distribution on to the t_{CsI} axis.

inefficiency due to the punch-through thus obtained from an EGS calculation.

3.3. Detection inefficiency due to the photonuclear interaction

The late cluster may include the photonuclear interaction events. Fig. 13 shows time spectra measured with the PSD modules for the LS (t_{PSD}), where, Fig. 13(a) is the t_{PSD} spectrum for the γ rays and neutrons from an Am/Be source, Fig. 13(b) for the events in the peak region, and Figs. 13(c) and (d) for the events with $-1\ \text{ns} < t_{CsI} < 2\ \text{ns}$ and $-4\ \text{ns} < t_{CsI} < -1\ \text{ns}$ in the tail region, respectively. A clear enhancement is observed in Fig. 13(c) at a large t_{PSD} where neutron signals are expected to exist according to the monitor data using the Am/Be source. The late cluster largely contains neutron signals which are generated by photonuclear interactions. The early cluster which has been explained as an electromagnetic cascade shower effect near to the punch-through can be surely eliminated by selecting the large t_{PSD} events as shown in Fig. 13(c). Thus, we can conclude that the photonuclear interaction can be cleanly picked up by the requirement for large t_{PSD} in the tail region. Another important point is that the requirement reduces the miss-tagging rate down to the level of accidental coincidence.

In order to achieve a tighter neutron call we place generous criteria on the PSD, ADC (a_{LS}) and TDC (t_{LS}) values from the LS as $15\ \text{ns} < t_{PSD} <$

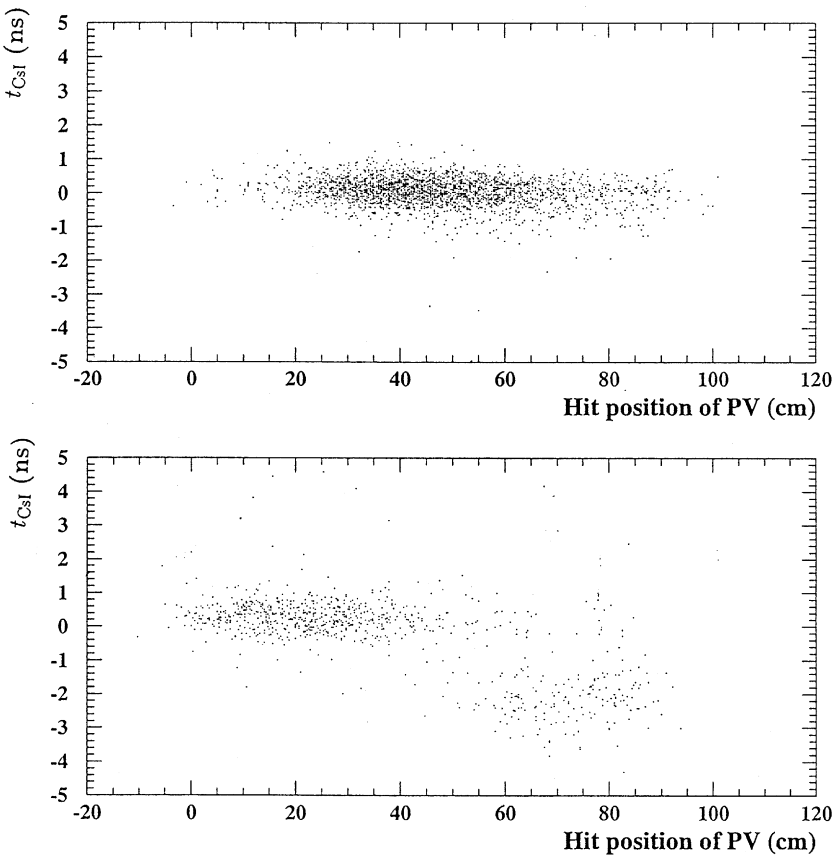

Fig. 10. Correlations between t_{CsI} and a hit position on PV, which are placed around the sample calorimeters, (a) for all events including the peak region and (b) for the events in the tail region. The CsI calorimeter 30-cm long is placed between 20-cm and 50-cm in the scale of abscissa.

50 ns, 0.1 MeV $< a_{LS} <$ 30 MeV and $t_{LS} <$ 30 ns, where a_{LS} is the electron-equivalent energy deposit in the LS.

The detection inefficiency of the CsI calorimeter due to the photonuclear interaction (DINEF) can be calculated as a ratio between the number of the events of $E_{CsI} < 1$ MeV with the neutron call ($N(E_{CsI} < 1$ MeV$:n)$) and that of all events (N(all)) using

$$\mathrm{DINEF} = \frac{N(E_{CsI} < 1 \text{ MeV}:n)}{N(\mathrm{all})} \frac{1}{\eta_{LS}}, \quad (1)$$

where η_{LS} is the neutron detection efficiency of the LS.

$N(E_{CsI} < 1$ MeV$:n)$ is estimated from the E_{CsI} distributions with the neutron call, which are shown in Fig. 14, as a mean value of the content of the bin of $E_{CsI} < 10$ MeV for each of eight E_γ bins. Fig. 15 shows the E_{CsI} distribution below 10 MeV summed up over the entire E_γ region as a check. It is consistent to be flat with E_{CsI} within the statistical error. The mean value for $E_{CsI} < 10$ MeV is indicated by the solid line. N(all) is the total number of events including the peak region in each E_γ bin without the neutron call.

The neutron detection efficiency of the LS, η_{LS}, is estimated from the multiplicity (m_{LS}) distribution of neutron hits. Since events of the zero-multiplicity that corresponds to the no-use of the LS cannot be

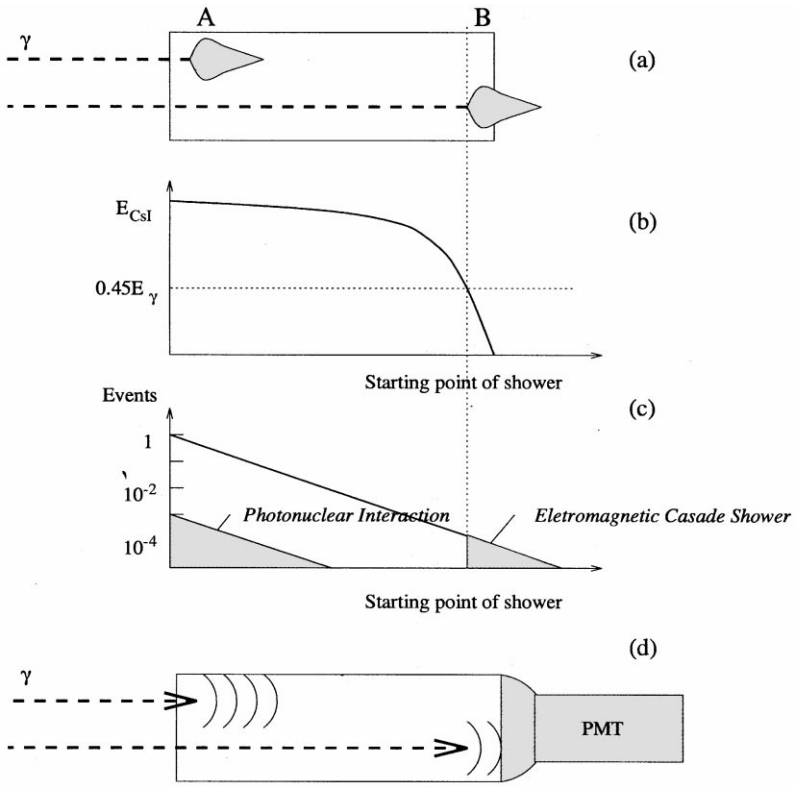

Fig. 11. Explanation of the two-clusters in the tail region: (a) a general feature of the cascade showers whose starting points are shown by A (an ordinary point) and B (an very deep point), (b) a shower-start-point dependence of the energy deposit in CsI (E_{CsI}), (c) the attenuation of the incident photons (Two shaded areas correspond to the events remaining in the tail region.), and (d) the behavior of the light propagation in the calorimeter.

directly counted without noise, η_{LS} is estimated from a Poisson distribution reproducing the data of $m_{LS} \geqslant 1$. The Poisson distribution reproduces well the data at every E_γ bin as shown in Fig. 16, in which the whole data in the tail region ($E_{CsI}/E_\gamma < 0.45$) are used. Then, the detection efficiency is given by $1 - \exp(-\mu)$, where the μ is the mean value of the Poisson distribution. An E_γ dependence of the μ is shown in Fig. 17.

The detection inefficiency of the CsI calorimeter due to the photonuclear interaction, DINEF, is listed in Table 1 and shown in Fig. 18. The detection inefficiency monotonically decreases with photon energy from 1×10^{-5} to 1×10^{-6} in the range 185–505 MeV.

4. Checks of the results for the CsI calorimeter

4.1. Neutron detection efficiency of the LS

The overall neutron detection efficiency, η_{LS}, given in Eq. (1) is estimated using the whole data in the tail region ($E_{CsI}/E_\gamma < 0.45$). It is implicitly assumed that the efficiency does not depend on E_{CsI}/E_γ, but in fact the η_{LS} (and μ) may depend on the process such as the multiplicity of neutrons and their energies. If the process largely changes with E_{CsI}, the μ may vary with E_{CsI}/E_γ. We examine the variation of the μ with E_{CsI}/E_γ, and find no significant dependence on E_{CsI}/E_γ except for a systematic E_γ difference, which is already folded in the

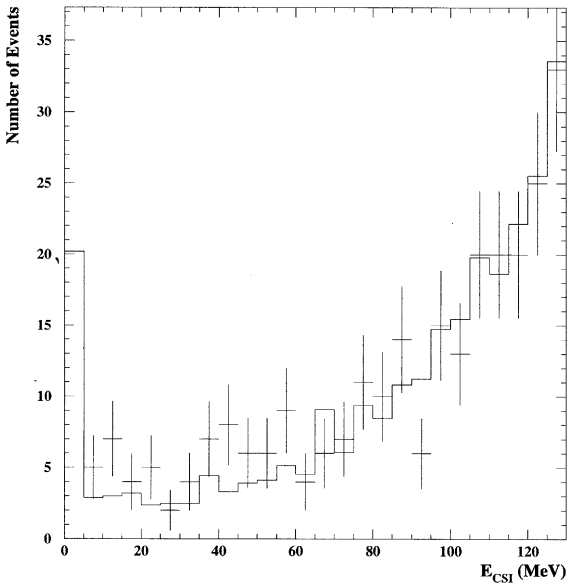

Fig. 12. E_{CsI} distribution in the tail region: the data with error bars are for the events having early timings (-4 ns $< t_{CsI} < -1$ ns), and the histogram shows an EGS calculation.

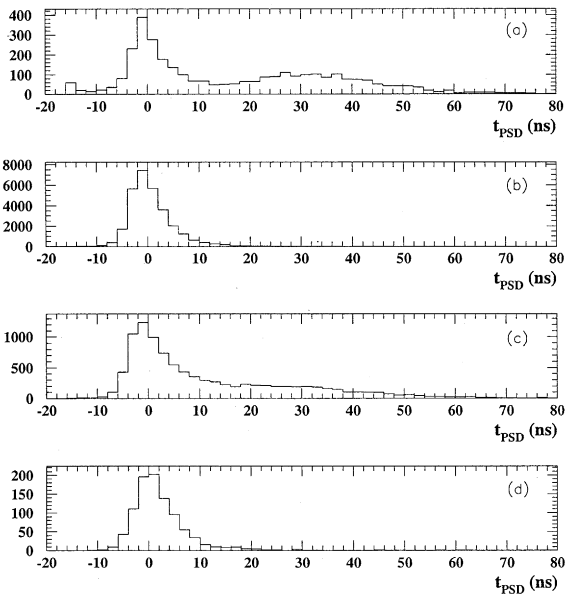

Fig. 13. Time spectra measured with PSD (Pulse Shape Discriminator, CAMBERA-2160) for (a) the monitor data using an Am/Be source; the peak at $t_{PSD} \simeq 0$ corresponds to γ rays and the bump above 10 ns to neutrons, (b) the events in the peak region, (c) the tail region events with -1 ns $< t_{CsI} < 2$ ns and (d) those with -4 ns $< t_{CsI} < -1$ ns.

Table 1
Detection inefficiencies of the CsI calorimeter

Photon energy (MeV)	Inefficiency (punch-through) ($\times 10^{-5}$)	Inefficiency (photonuclear) ($\times 10^{-5}$)
205	2.75 ± 0.37	1.11 ± 0.15
245	1.40 ± 0.26	1.12 ± 0.15
285	1.10 ± 0.23	0.71 ± 0.13
325	1.75 ± 0.30	0.81 ± 0.15
365	1.00 ± 0.22	0.39 ± 0.11
405	1.40 ± 0.26	0.37 ± 0.12
445	0.90 ± 0.21	0.21 ± 0.09
485	1.00 ± 0.22	< 0.13

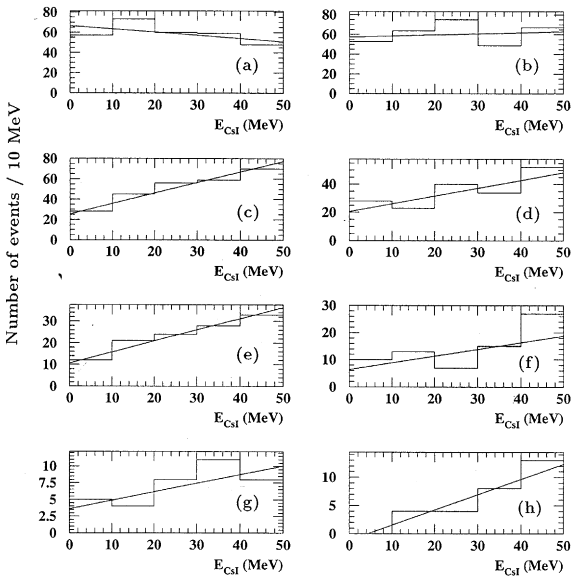

Fig. 14. E_{CsI} distributions with the neutron-call in the various photon energy ranges (a)–(h): for E_γ of every 40 MeV bin from 185 MeV to 505 MeV. A straight line fit to the data is shown as an eye guide.

estimation of the neutron detection efficiency, as shown in Fig. 19.

As an over-all check we take a ratio between the number of the events with neutron signals in the tail region and the total number of events. The E_γ dependence of the ratio divided by the η_{LS} is shown in Fig. 20. The curve represents the ratio between the cross sections of the photonuclear interaction and

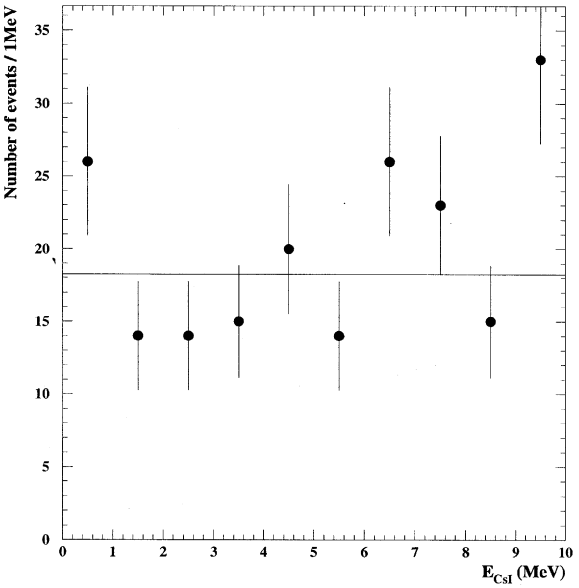

Fig. 15. E_{CsI} distribution with the neutron-call for all E_γ events. The mean value is indicated by the solid line.

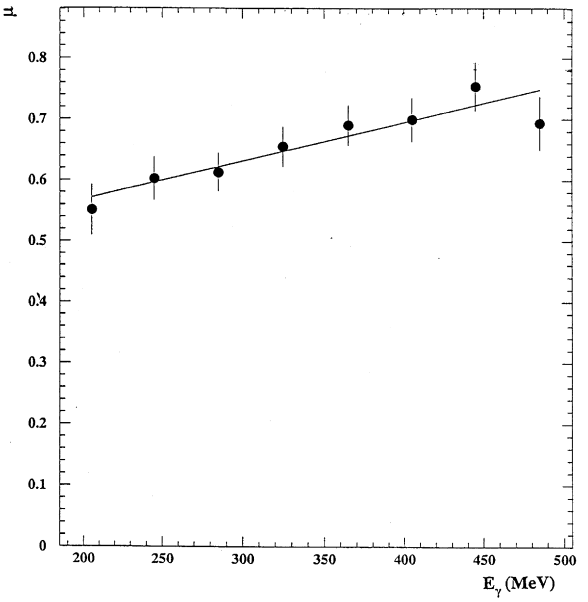

Fig. 17. E_γ dependence of the mean value (μ) of the Poisson distribution fitted to m_{LS} distributions.

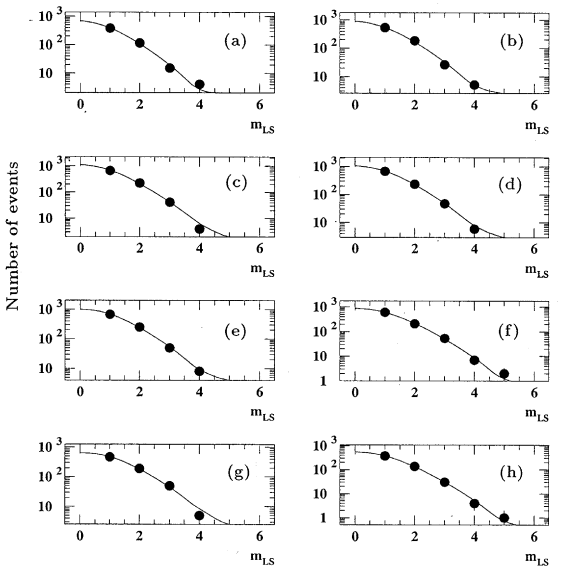

Fig. 16. Multiplicity distributions of the LS with neutron signal (m_{LS}): (a)–(h) are those for the tail ($E_{\mathrm{CsI}}/E_\gamma < 0.45$) events in every 40 MeV bin of E_γ from 185 MeV to 505 MeV. The curves are the Poisson distribution fit to the data of $m_{\mathrm{LS}} \geqslant 1$.

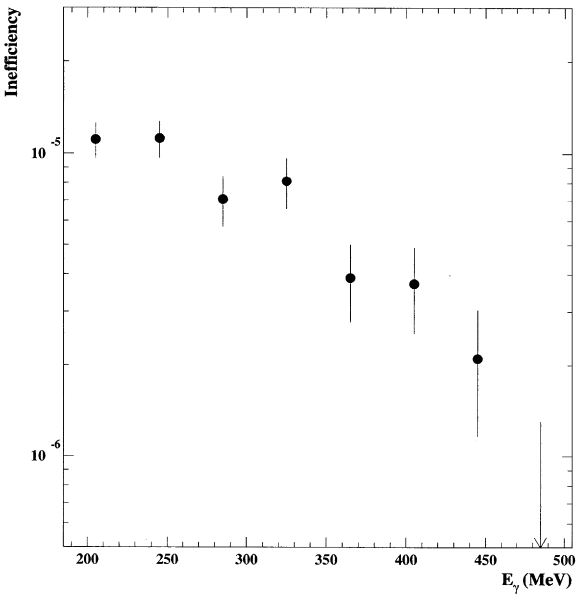

Fig. 18. Detection inefficiency of the CsI calorimeter due to the photonuclear interaction. The error includes the error of the neutron detection efficiency as well as the statistical fluctuation of the $E_{\mathrm{CsI}} < 1$ MeV events. At the highest energy point the start-point of the arrow shows the upper limit value with a 90% confidence level (2.3 events in the 0–10 MeV bin in Fig. 14(h)).

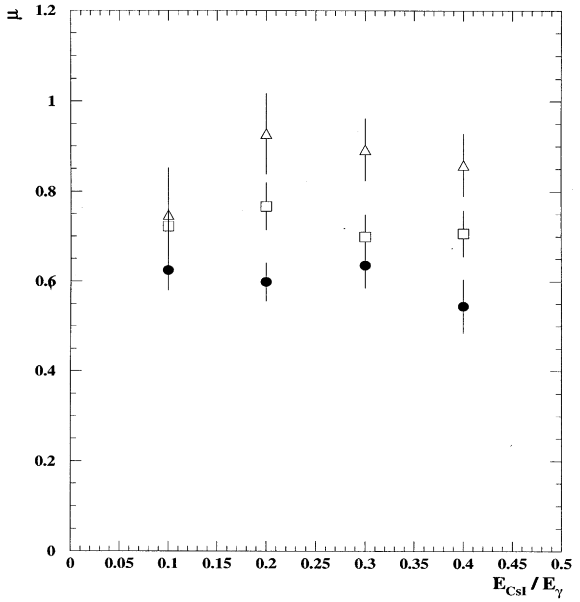

Fig. 19. The variation of μ for different E_γ and E_{CsI}/E_γ samples. The ●, □ and △ are the μ values obtained in the regions $E_\gamma = 250 \pm 50$ MeV, 350 ± 50 MeV and 450 ± 50 MeV, respectively, and the E_{CsI}/E_γ range is ± 0.05.

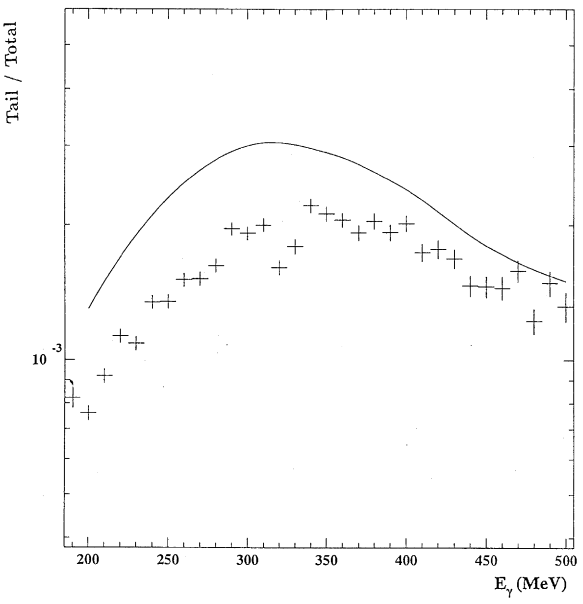

Fig. 20. Photon-energy dependence of the ratio of the number of events in the tail and total E_{CsI} regions (Tail/Total). The tail events are those with measured neutron signals, and the ratio is corrected for the neutron detection efficiency. The curve is calculated from the ratio of photonuclear and electromagnetic-cascade cross sections.

the electromagnetic cascade shower process, where we estimate the photonuclear interaction cross section by using the data of Be target [8] with an assumption of the A^1 dependence (where A is the mass-number of the target nucleus) and the cross section of the electromagnetic cascade shower process is calculated with EGS. The data and the curve show a good resemblance typical in the bump due to the Δ resonance, and it indicates us a good identification of the photonuclear interaction. For a quantitative comparison we should know the fraction which may arise due to the partial selection of the tail region ($E_{CsI}/E_\gamma < 0.45$) and its E_γ dependence.

For one-third of the running time we took data at a different position of the CsI calorimeter relative to the LS (30-cm downstream of the normal position shown in Fig. 4). If the reactions were different between the zero and the other tail regions, for example, the main contribution for $E_{CsI} < 1$ MeV were a one-step violent reaction $A(\gamma,n's)A'_{gs}$ not like the evaporation in the tail region, the geometrical acceptance for those neutrons (the former go more forward than the latter) might change by the CsI position relative to the LS. No significant difference between the two runs is observed in the final values of the detection inefficiency, and we combine them in the analysis.

4.2. Accidental background

The accidental rate between the tagging and neutron signals is given as $\tau \dot{N}_{LS} \dot{N}_{Tag}$, where τ is the time window for neutron signals, $\dot{N}_{LS}$ the rate of neutron signals and $\dot{N}_{Tag}$ the rate of all tagging counters. Since the signal rate is almost equal to $\dot{N}_{Tag}$, the contamination by the accidental coincidence (noise-to-signal ratio) is expressed as $\tau \dot{N}_{LS}$. Taking the values of the $\tau = 30$ ns and $\dot{N}_{LS} \leqslant 6$ Hz (the instantaneous rate of LS is about 0.6 kHz for the discriminator threshold of 0.1 MeV and a fraction of neutron signals is less than 0.01), the contamination is less than 1.8×10^{-7}. However, another factor of 0.01 exists thanks to the small miss-tagging rate, because most of tag-signals associate with the photon and they do not contribute to the detection inefficiency. Then the accidental background is expected to be less than 1.8×10^{-9}. It is negligibly

small for the present evaluation of the detection inefficiency, even if we consider the maximum change of the duty factor from 10% to 3% (the instantaneous rate would be increased by a factor of three). The probability of an accidental overlap to the signal of $E_{CsI} < 1$ MeV, which makes the detection inefficiency to be underestimated, is also negligibly small, because the CsI-ADC gate time of 100 ns is already very short against the rate of CsI which is estimated to be a few kHz above the threshold of 1 MeV based on the $1/E_\gamma$ spectrum.

5. Results for the sandwich calorimeter

Based on the study of the CsI calorimeter, the punch-through effect for the sandwich calorimeter is estimated from an EGS calculation. The sampling effects due to the electromagnetic cascade shower are included in the calculation, because the events with a none-or-small energy deposit ($E_{Sand} < 1$ MeV) are selected in the calculation regardless of the process as the factor which contributes to the detection inefficiency. The result is listed in Table 2. The detection inefficiency due to the photonuclear interaction of the sandwich calorimeter is obtained from the events with neutrons in the same way as that of the CsI calorimeter.

Fig. 21 shows the E_{Sand} distributions for the events with neutron signals in the various E_γ regions. In contrast to the E_{CsI} distribution there are enhancements at low deposit energy, which must be due to the sampling effect that does not exist in the case of the CsI calorimeter. The detection inefficiency is obtained from the zero($E_{Sand} < 1$ MeV)-to-total ratio with a correction for the neutron detection efficiency which is obtained from a Poisson fit using the m_{LS} data in the runs for the sandwich calorimeter. The E_γ dependence of the detection inefficiency due to the photonuclear interaction is listed in Table 2 and is shown in Fig. 22. The obtained inefficiency values are larger than those of the punch-through and the sampling effect due to the electromagnetic cascade shower process.

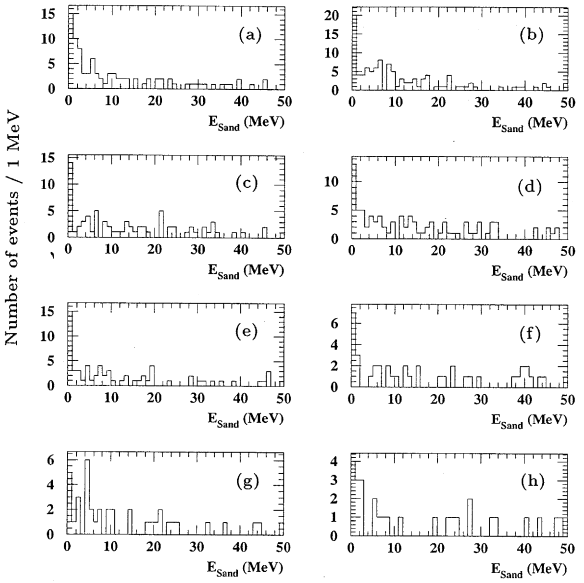

Fig. 21. E_{Sand} distributions with the neutron-call for the data in every 40 MeV bin of E_γ from 185 MeV to 505 MeV ((a)–(h)).

Table 2
Detection inefficiencies of the lead-scintillator sandwich calorimeter

Photon energy (MeV)	Inefficiency (EM-cascade) ($\times 10^{-5}$)	Inefficiency (photonuclear) ($\times 10^{-4}$)
205	4.7 ± 1.0	1.15 ± 0.30
245	3.5 ± 0.5	1.72 ± 0.39
285	2.5 ± 0.4	1.49 ± 0.40
325	2.1 ± 0.4	1.62 ± 0.45
365	2.0 ± 0.3	2.32 ± 0.60
405	2.0 ± 0.3	1.22 ± 0.46
445	2.1 ± 0.3	0.99 ± 0.44
485	2.3 ± 0.4	1.13 ± 0.57

The detection inefficiency of the sandwich calorimeter is regarded to be dominated by the sampling effect caused by photonuclear interactions: the detection inefficiency arises when all of the charged particles produced by photonuclear interactions are absorbed in lead. Therefore, the converter (lead) should be thinner in order to reduce the detection inefficiency. For more understanding about the sandwich calorimeter a further experimental studies for the calorimeters having various converter thicknesses are necessary.

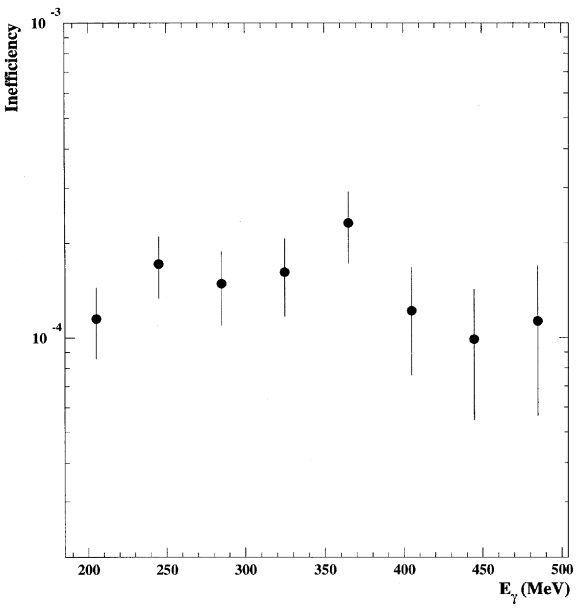

Fig. 22. Detection inefficiency of the lead-scintillator sandwich calorimeter due to the photonuclear interactions. The error comes from the uncertainty in the neutron detection efficiency as well as the statistical fluctuation of the $E_{\mathrm{Sand}} < 1$MeV events.

6. Summary

By analyzing the events in the low energy-deposit (tail) region for the CsI calorimeter 30-cm long, the estimation of the punch-through using the EGS code is confirmed to be correct.

The other source of the detection inefficiency, the photonuclear interactions, is identified by requiring neutron hits in the surrounding liquid-scintillation counters. The detection efficiency for neutrons of the liquid scintillation counters, which is the most important correction, is estimated from the Poisson distribution fit to the multiplicity distribution of the neutron hits. The obtained values of the efficiency are considerably large. This is due to the fact that a large number of neutrons (more than ten) are produced in a photonuclear interaction. The tail-to-total ratio shows the E_γ dependence consistent with that of the cross-section ratio between photonuclear interaction and electromagnetic cascade shower process obtained from previous experimental data. The obtained inefficiency due to the photonuclear interaction shows a monotonic decrease with energy and it is less than 1×10^{-5} above 300 MeV.

The result for the lead-scintillator sandwich counter indicates that the dominant process is the sampling effect after photonuclear interactions and that the detection inefficiency is as large as 1×10^{-4}. A further experimental study would be necessary to optimize the converter thickness.

Acknowledgements

The authors thank the operating crew of the INS-ES for their support during the present experiment.

References

[1] T. Inagaki et al., KEK Internal 96-13 (KEK-PS-E391 Proposal), 1996.
[2] T. Inagaki et al., Nucl. Instr. and Meth. A 359 (1995) 478.
[3] W.R. Nelson, H. Hirayama, D.W.O. Rogers, SLAC Rep. 265 (1985).
[4] A. Leprêtre et al., Nucl. Phys. A 367 (1981) 237.
[5] J. Ahrens et al., Nucl. Phys. A 251 (1975) 479.
[6] S. Arai et al., Jpn. J. Appl. Phys. 14 (1975) 95.
[7] M. Mutoh, J. Sci. Hiroshima Univ. 51 (1987) 187.
[8] P. Carlos et al., Nucl. Phys. A 431 (1984) 573.